

Park K. Kim D.-H. Lee K.-S. Lee W.-J. and Kim S.-J. 'Preparation and photocatalytic activity of nanotubes obtained from titanium dioxide'. Science Direct 2008; 3-14.

11 P.E. Agbo 'ON The Effect of Temperature on Thickness and Bandgap $\text{TiO}_2/\text{Fe}_2\text{O}_3$ CORE-SHELL Crystalline thin film' Journal of Ovonic Research Vol. 9, No. 4, July - August 2013, p. 105 - 112

12 F. W. Mont. J. K. Kim. Martin F. Schubert. E. Fred Schubert and R. W. Siegel 'High-refractive-index TiO_2 -nanoparticle-loaded encapsulants for light-emitting diodes' JOURNAL OF APPLIED PHYSICS. 2008. 103. 083120.

show the suitability of the deposited films for using them in optoelectronic devices and solar cells.

References

1 A. G. Sagesh, P.Z. Ketan, P.G. Dipak, 'Effect of Thermal Annealing on Optical and Band gap of chemically deposited $\text{TiO}_2/\text{Fe}_2\text{O}_3$ Core/shell Oxide Thin Films' *Advances in Applied Science Research*, 2011, 2 (6), 393-399

2 W. A. Kozuka H. Photoanodic Properties of Sol-Gel-Derived Fe_2O_3 Thin Films Containing Dispersed Gold and Silver Particles'. *J. Phys. Chem. B* 2003; 107: 12713.

3 A. P.E. Effect of Thermal Annealing on Optical and Band gap of chemically deposited $\text{TiO}_2/\text{Fe}_2\text{O}_3$ Core/shell Oxide Thin Films *Advances in Applied Science Research*, 2011, 2 (6), 393-399

4 18) O. F. Caltun, "Pulsed Laser Deposition of NiFe_2O_4 Thin Films", *Journal of Optoelectronics and Advanced Materials*, Vol.6, No.3, 2004, pp. 935 – 938.

5 R. Dom, G. Siva Kumar, H.G. Kim, Sh. V. Joshi, A. S. Chary and P. H. Borse, 'Design and development of ferrite composite

film electrode for photoelectrochemical energy application' *Materials Science Forum* Vol. 781 (2014) pp 45-61

6 A. Abdulwahhab Ali, "Structural, Optical and electrical properties of ZnO , GaO GeO_2 thin films", MSc thesis, University of Baghdad, 2013, p p.34.

7 J. I Peña-Flores, A. F Palomec-Garfias, C. Márquez-Beltrán, E. S.-Mora, Estela G.-Barojas and F. P.-Rodríguez, 'Fe effect on the optical properties of $\text{TiO}_2/\text{Fe}_2\text{O}_3$ nanostructured composites supported on SiO_2 microsphere assemblies' *Nanoscale Research Letters* 2014, 9, 499.

8 M. I. Pownceby, Michael J. Fisher-White, and Varghese Swamy 'Phase Relations in the System $\text{Fe}_2\text{O}_3+\text{Cr}_2\text{O}_3+\text{TiO}_2$ between 1000 and 1300°C and the Stability of $(\text{Cr,Fe})_2\text{Ti}_{2n-1}\text{O}_{2n-1}$ Crystallographic Shear Structure Compounds' *Journal of Solid State Chemistry* 161, 45-56 (2001)

9 Xing M. Zhang, J. Chen, F. Photocatalytic Performance of N-Doped TiO_2 Adsorbed with Fe^{3+} Ions under Visible Light by a Redox Treatment. *Journal of Physical Chemistry* 2009; 113, 12848–12853.

10 Q. M. Yoon, C.-R. Oh, H.-J. Lee, N.-H.

The real ϵ_r and imaginary ϵ_i parts of the dielectric constant for $\text{TiO}_2/\text{Fe}_2\text{O}_3$ films were determined by formula $\epsilon_r = n^2 - k^2$ and $\epsilon_i = 2nk$. The variation of the real (ϵ_r) and imaginary (ϵ_i) parts of the dielectric constant for different film thicknesses are illustrated in figures (8,9). The figures revealed that the values of the real part are higher than that of the imaginary part. It is observed from the figs. that the real and imaginary dielectric constants decrease with the increase of the wavelength of the incident radiation and this behavior is due to the change of reflectance and absorbance.

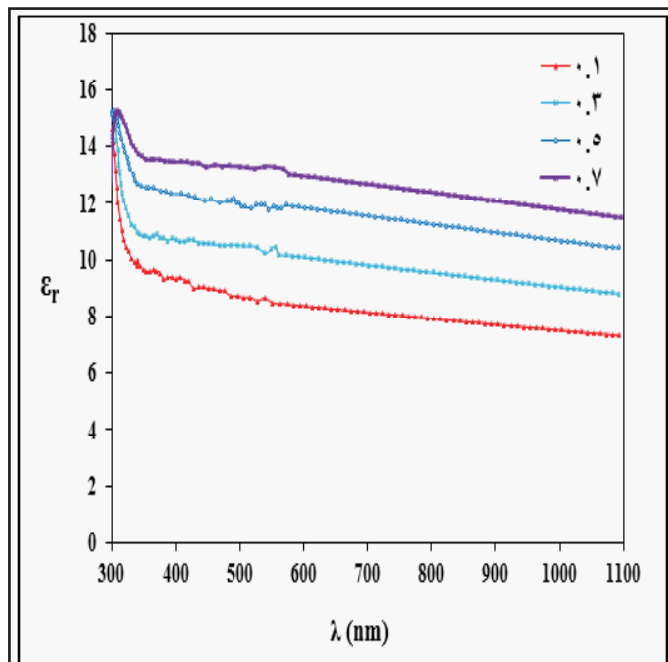


Fig.8. Real part of dielectric constant for $\text{TiO}_2/\text{Fe}_2\text{O}_3$ films

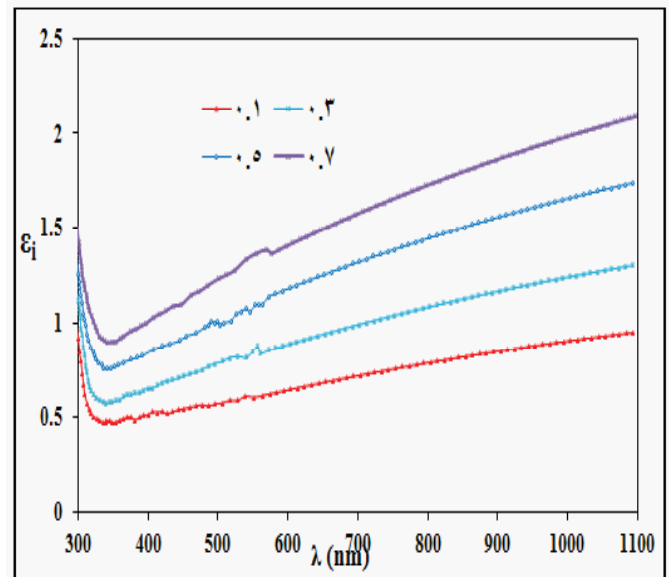


Fig.9. Imaginary part of dielectric constant for $\text{TiO}_2/\text{Fe}_2\text{O}_3$ films

4-CONCLUSIONS

In this work, $\text{TiO}_2/\text{Fe}_2\text{O}_3$ films of different TiO_2 content have been prepared by pulse laser deposition technique onto glass substrate. The films show direct band gap in the range 3.3 –4 eV. The films exhibit high absorbance in the UV region from ~ 300 nm to 1100 nm. And low absorbance in the visible / near infrared region from ~ 300 nm to 1100 nm. Variations in the optical constants with wavelength are found to be TiO_2 content dependent of the films. The optical properties refractive index, optical band gap and low dielectric constant of the as-deposited films

Fig.6. shows the variation of refractive index as a function of the wavelength for TiO₂/Fe₂O₃ films. It is found from this fig.4. That the refractive index decreases with the increasing of wavelength of the incident photon. The value of refractive index for TiO₂/Fe₂O₃ films it is found from this fig.(6) that increases with the increase TiO₂ content. From the figure it is evident that the refractive index increases from 3.65 to 3.95 with the increase of TiO₂ of the film which is in good agreement with those reported by other researchers.

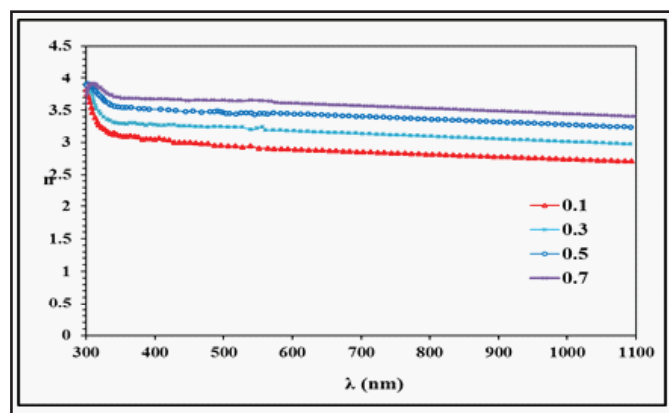


Fig. (6) The Refractive index versus wavelength of incident radiation for TiO₂/Fe₂O₃ films

The behavior of extinction coefficient is nearly similar to the corresponding absorption coefficient; the variation of extinction coefficient for TiO₂/Fe₂O₃ films with wavelength is shown in figure 7. It is observed that

the extinction coefficient decreases with the increase of the TiO₂ contents. The rise and fall in the extinction coefficient is directly related to the absorption of light. as shown in fig.(7) for TiO₂/Fe₂O₃ films at different extinction coefficient from fig.(5), we can observed that the extinction coefficient for TiO₂/Fe₂O₃ films increases with increasing the extinction coefficient (12) .

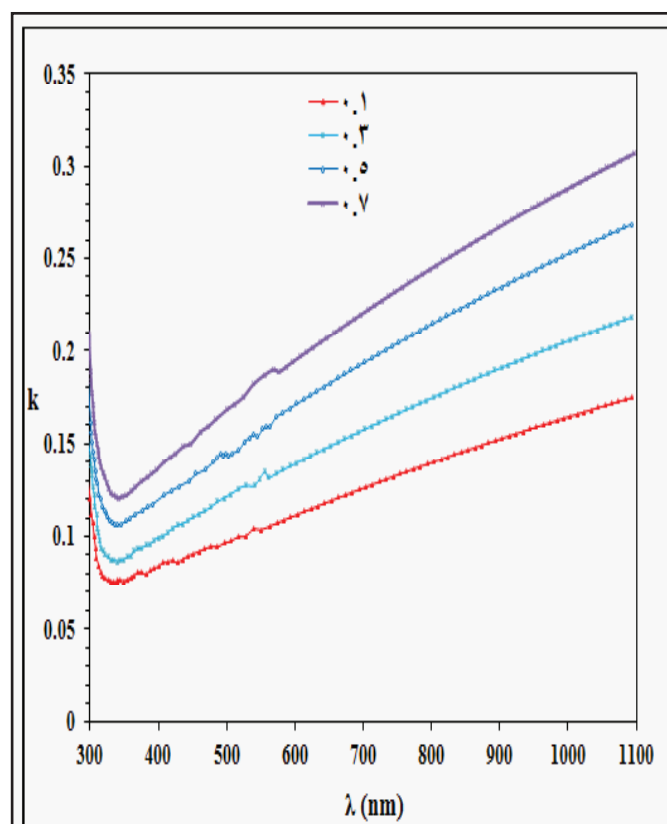


Fig.(7). The Extinction coefficient versus wavelength of incident radiation for TiO₂/Fe₂O₃ films

The energy band gap can be estimated by assuming a direct transition between valence and conduction band of TiO₂/Fe₂O₃ film. In order to determine the direct optical band gap was used the relation as follows

$$\alpha h\nu = A(h\nu - E_g)^{1/2} \quad \dots(3)$$

Where A is a parameter independent of $h\nu$ and E_g is the optical band gap.

Plotting the dependence of $(\alpha h\nu)^2$ versus $h\nu$, the value of optical band gap can be determined by extrapolating the linear portion of this plot to $(\alpha h\nu)^2 = 0$. Such plots for representative TiO₂/Fe₂O₃ films are shown in Fig. 5. The obtained values of optical band gap: (3.3-4) eV for films deposited at 600 is in good agreement with those reported by other researchers [10,11]. The reduction in the optical band gap is probably due to the increase Absorption coefficient and modification of the ferrite structure.

the increase Absorption coefficient Hematite Iron(III) oxide.

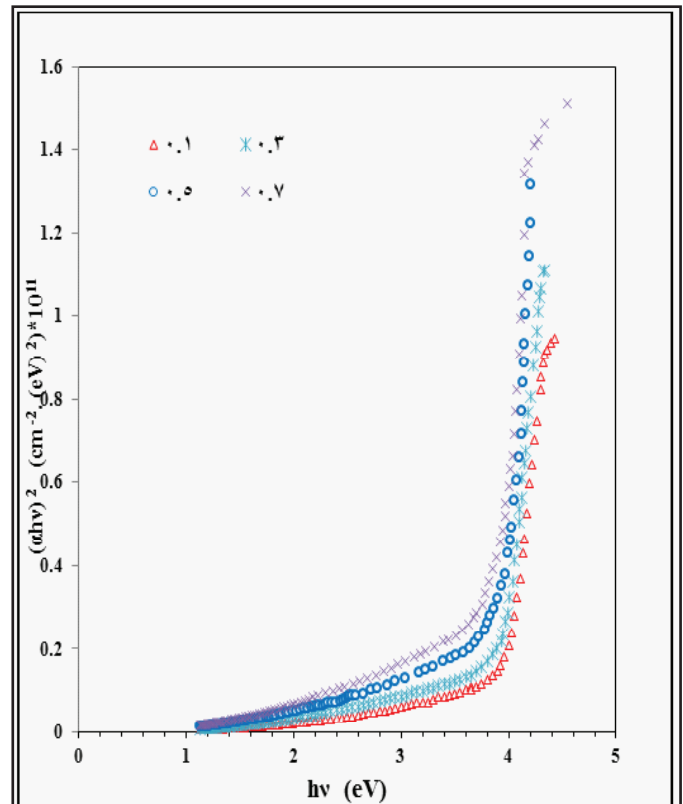


Fig. (5) The plot of $(\alpha h\nu)^2$ vs. $h\nu$ for TiO₂/Fe₂O₃ films

Optical properties for thin films

The spectral dependence of The optical trans - missions of TiO₂/Fe₂O₃ films with thickness 150nm are characterized by strong m at short wavelength region within the range (300-1100)nm. We can observe that from this figure(3) All specimens showed transmi - sion less than (60%) in the wavelength (300-500nm) and increment to reach to (66.94%) at (x=0.1) in the wavelength (1100nm). In general, it may be observed from Fig (1) that transmittance decreases with increasing of TiO₂ content.

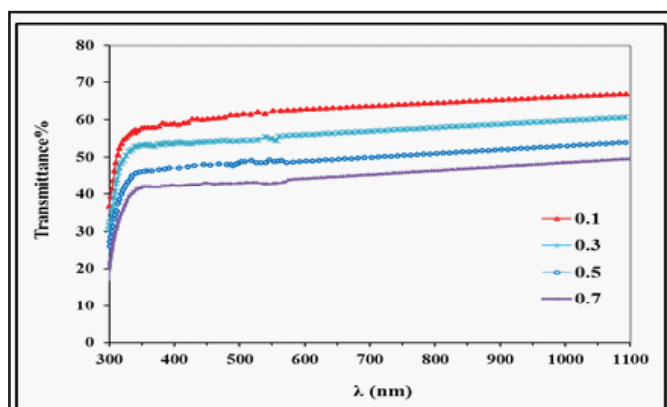


Fig. (3) The Transmittance spectra for TiO₂/Fe₂O₃ films

The absorption coefficient (α) of TiO₂/Fe₂O₃ films prepared by using pulse laser deposition technique are determine from the region of high absorption at the fundamental absorption edge of film. The absorption coe - ficient (α) was calculating using using la - bert law equation (1)

$$\ln = 2.303 A = \alpha t \quad \dots\dots\dots(2)$$

Where:

I_0 and I_t are the incident and transmitted light respectively.

A_t is the optical absorbance and (t) is the film thickness.

Fig.4 shows the absorption coefficient as a function of wavelength. From this figure, TiO₂/Fe₂O₃ film exhibits a strong absor - tion of photons at the short wavelength r - gion ($\lambda=320$ nm) in the region.

It could be observed that the absorption coefficient increases with increasing wav - length due to decrease in transmittance. The maximum value of absorption coefficient at (x=0.7) which is value reach to (76602.8 cm⁻¹). In general, it may be observed that the absorption coefficient increases with i - creasing of TiO₂ content.

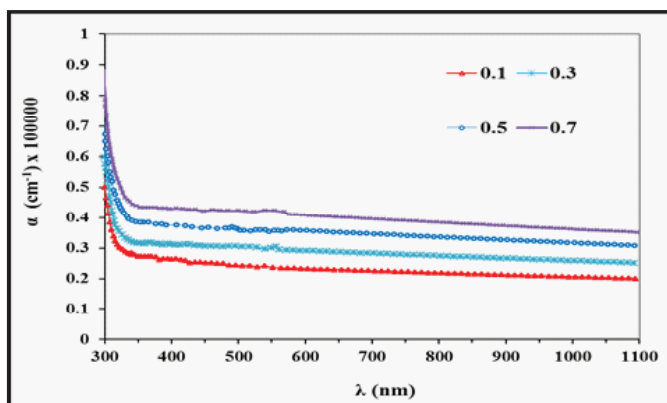


Fig. (4) The absorbance spectra for TiO₂/Fe₂O₃ films

correspond miller indices (110) referred to the TiO₂ while the other one (110) referred to the ferric oxide (7).

The XRD spectra data of TiO₂/Fe₂O₃ film presence of Miller indices corresponding to (110) and (211) major lattice planes identified by the consultation of powder diffraction file card no. 230-0296. Additionally, minor lattice planes of (311), and (220) were present (8, 9). A point of interest is that the preferential orientation is the (110) direction at

($2\theta=27.4^\circ$) of the films and this may be due to the layer stability of the (220) planes which reflects the more relaxed bonds with minimum energy. Table (1) presents the experimental and the standard values (from International Centre for Diffraction Data) for TiO₂/Fe₂O₃ thin films with different (TiO₂) content.

Table (1): X-ray diffraction spectra data for TiO₂/Fe₂O₃ thin films with different TiO₂ content.

TiO ₂ ratio	2 θ (Deg.)	FWHM (Deg.)	d _{exp} (Å)	G.S (nm)	d _{std} (Å)	hkl	phase	card No.
0.1	24.1739	0.2484	3.6787	32.7	3.6832	(110)	Fe ₂ O ₃	96-101-1268
	27.4037	0.5466	3.2520	15.0	3.2448	(110)	TiO ₂	96-410-2356
	33.2671	0.2981	2.6910	27.8	2.7010	(211)	Fe ₂ O ₃	96-101-1268
	35.6025	0.2484	2.5197	33.6	2.5174	(101)	Fe ₂ O ₃	96-101-1268
	39.4286	0.2981	2.2835	28.3	2.2938	(222)	TiO ₂	96-410-2356
	40.9689	0.4969	2.2011	17.1	2.2070	(210)	Fe ₂ O ₃	96-101-1268
	45.0435	0.2981	2.0110	28.8	2.0522	(120)	TiO ₂	96-410-2356
	49.5652	0.3975	1.8377	22.0	1.8416	(202)	Fe ₂ O ₃	96-101-1268
	54.0870	0.5963	1.6942	15.0	1.6955	(312)	Fe ₂ O ₃	96-101-1268
	57.7640	0.7950	1.5948	11.4	1.6003	(332)	Fe ₂ O ₃	96-101-1268
0.3	24.2733	0.1988	3.6638	40.9	3.6832	(110)	Fe ₂ O ₃	96-101-1268
	27.6522	0.3478	3.2233	23.5	3.2448	(110)	TiO ₂	96-410-2356
	33.3665	0.2484	2.6832	33.4	2.7010	(211)	Fe ₂ O ₃	96-101-1268
	35.8509	0.2981	2.5028	28.0	2.5174	(101)	Fe ₂ O ₃	96-101-1268
	39.6273	0.3478	2.2725	24.3	2.2938	(222)	TiO ₂	96-410-2356
	41.1180	0.4472	2.1935	19.0	2.2070	(210)	Fe ₂ O ₃	96-101-1268
	45.1925	0.2981	2.0048	28.9	2.0522	(120)	TiO ₂	96-410-2356
	49.6149	0.2981	1.8359	29.4	1.8416	(202)	Fe ₂ O ₃	96-101-1268
	54.1863	0.2981	1.6913	29.9	1.6955	(312)	Fe ₂ O ₃	96-101-1268
	57.8634	0.3478	1.5923	26.1	1.6003	(332)	Fe ₂ O ₃	96-101-1268
0.5	24.4224	0.2484	3.6418	32.7	3.6832	(110)	Fe ₂ O ₃	96-101-1268
	27.7019	0.2484	3.2177	32.9	3.2448	(110)	TiO ₂	96-410-2356
	33.4161	0.2484	2.6793	33.4	2.7010	(211)	Fe ₂ O ₃	96-101-1268
	35.9503	0.1988	2.4961	42.0	2.5174	(101)	Fe ₂ O ₃	96-101-1268
	36.1230	0.1843	2.4845	45.3	2.4860	(101)	TiO ₂	96-410-2356
	39.6770	0.3975	2.2698	21.2	2.2938	(222)	TiO ₂	96-410-2356
	41.4658	0.4472	2.1759	19.0	2.1858	(111)	TiO ₂	96-410-2356
	45.2919	0.1988	2.0006	43.3	2.0522	(120)	TiO ₂	96-410-2356
	49.6646	0.2981	1.8342	29.4	1.8416	(202)	Fe ₂ O ₃	96-101-1268
	54.5839	0.3975	1.6800	22.5	1.6860	(211)	TiO ₂	96-410-2356
0.7	56.8696	0.3478	1.6177	26.0	1.6224	(220)	TiO ₂	96-410-2356
	57.9130	0.2981	1.5910	30.5	1.6003	(332)	Fe ₂ O ₃	96-101-1268
	24.2236	0.2981	3.6712	27.3	3.6832	(110)	Fe ₂ O ₃	96-101-1268
	27.5031	0.2484	3.2405	32.9	3.2448	(110)	TiO ₂	96-410-2356
	33.2671	0.2484	2.6910	33.4	2.7010	(211)	Fe ₂ O ₃	96-101-1268
	35.7516	0.2484	2.5095	33.6	2.5174	(101)	Fe ₂ O ₃	96-101-1268
	36.1988	0.1988	2.4795	42.1	2.4860	(101)	TiO ₂	96-410-2356
	41.2671	0.2484	2.1859	34.2	2.1858	(111)	TiO ₂	96-410-2356
	45.1429	0.1988	2.0069	43.3	2.0522	(120)	TiO ₂	96-410-2356
	49.5155	0.3478	1.8394	25.2	1.8416	(202)	Fe ₂ O ₃	96-101-1268
	54.4348	0.2484	1.6842	36.0	1.6860	(211)	TiO ₂	96-410-2356
	56.7205	0.2484	1.6216	36.3	1.6224	(220)	TiO ₂	96-410-2356

Sample preparation

Ferrites with general formula $\text{TiO}_2/\text{Fe}_2\text{O}_3$ (where $x=0.1, 0.3, 0.5$, and 0.7), were prepared by PLD technique. Nano Powders of Fe_2O_3 and TiO_2 were weighed and mixed according to the general composition formula by moles ratio. The powders were mixed and blended homogenously through dry mixing using a ball mill. After powder mixture, they were pressed using a die with diameter (1cm) to produce specimens in a pellet shape. The pressing load used was (3 ton) and the specimen held for 1min under pressure using a hydraulic press (of a maximum load 15 ton). The specimens were then sintered at 900°C for two hours and then left to cool down to room temperature. Ferrite thin films were prepared by pulse laser deposition. An incident beam of Nd:YAG SHG Q-switched laser was focused on the target surface to make an angle of (45°) with it. The films were deposited on glass substrates at room temperature. The characteristics of laser source are ($\lambda=1064\text{nm}$), energy 900mJ, frequency 6Hz, distance between substrate and target 1cm with chamber pressure of ($6 \times 10^{-2}\text{mbar}$), and number of pulses 900. The films were annealed in an oven at a temperature of 600°C for 2hr. The spinel structure was characterized by x-ray diffraction carried out using Shimadzu XRD-6000 diffractometer with $\text{Cu K}\alpha$ radiation ($\lambda=1.5405\text{\AA}$) at scanning speed 5 deg/min. The Atomic Force Microscopy

(AFM) studies were performed on Angstrom Advanced Inc. 2008, USA. Scanning Electron Microscopy (SEM) studies were performed using (JOEL JSM-6400) with magnification 589 and 477. The optical Absorbance of the films was measured in the spectral range 300-1100nm, using UV spectrophotometer.

Thickness Measurement.

Film thickness measurements were done using optical interferometer method, by TF-C-UVIS-SR spectrometer test thickness range $20 \times 10^4 \text{\AA} - 50$. This method is based on interference of a light beam reflected from a thin film surface and substrate bottom, with error rate at 3%. He-Ne laser ($0.632\mu\text{m}$) as the light source was used and the thickness is determined using the formula:

$$t = \Delta x / x \times \lambda / 2 \quad \dots 1$$

Where (x) is the fringe width, (Δx) is the distance between two fringes and (λ) wavelength of laser light (6).

3. Results and discussion

X-ray Diffraction

Figure 1 shows XRD patterns of $\text{TiO}_2/\text{Fe}_2\text{O}_3$ where ($x=0.1, 0.3, 0.5$ and 0.7) prepared by PLD technique. The patterns were compared with standard data (96-230-0296) and the formation of single phase cubic spinel structure in all specimens was confirmed with the appearance of secondary phases. The component $\text{TiO}_2/\text{Fe}_2\text{O}_3$ were multi phases. The

1- Introduction

Among the various forms of iron oxides, maghemite ($\gamma\text{-Fe}_2\text{O}_3$) and hematite ($\alpha\text{-Fe}_2\text{O}_3$) are of great importance in technological and industrial applications (1, 2).

Among the transition metal oxide semiconductors, Fe_2O_3 has been one of the most extensively explored materials as a candidate electrode. Compared to other semiconductor materials, hematite ($\alpha\text{-Fe}_2\text{O}_3$) has many potential advantages. Maghemite has numerous applications like recording, memory devices, magnetic resonance imaging, drug delivery or cell targeting. Hematite exhibits high resistance to corrosion, therefore, it has been extensively used in many fields which include photo-anode for photo assisted electrolysis of water. It is an active component of gas sensors, catalyst, lithium ion battery, pigments and oxidizer in the maghemite composition. It is also used in magnetic fluids, also called ferrofluids, for damping in inertial motors, shock absorbers, heat transfer fluids (3).

Titanium oxide thin film has been one of the most extremely studied oxides because of its role in various applications namely photo-induced water splitting, dye synthesized solar cells, environmental purifications gas sensors display devices, batteries etc (4,5).

This study reports the synthesis of novel $\text{TiO}_2/\text{Fe}_2\text{O}_3$ thin film via pulse laser deposition technique. The effect of post

deposition annealing on the optical and electrical properties were also reported. For performance improvement was carried out with the nano-sized Fe_2O_3 thin layer Manufacturing Nanostructures.

2-Experimental

Raw material

Nano powder filler of Titanium oxide and Fe_2O_3 were supplied by Cristal Globa Phama Company with particle size 50 nm and 57nm is shown in Fig (1 and 2) respectively.

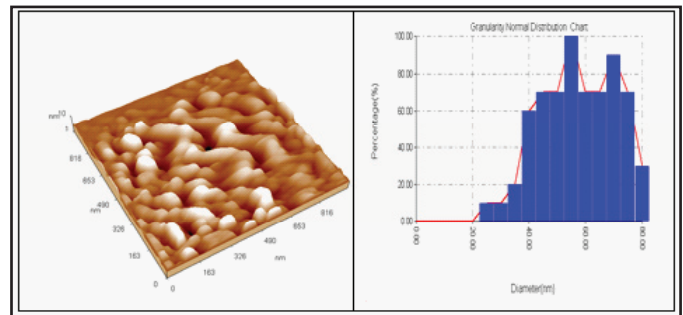


Fig (1): Granularity normal distribution chart for nano Fe_2O_3 particles

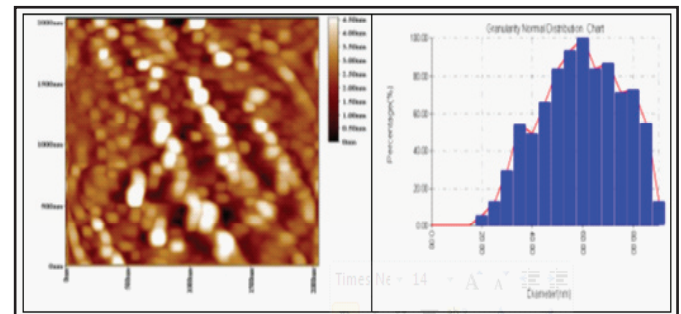


Fig (2): Granularity normal distribution chart for nano TiO_2 particles

Zaidoon T.Mohammed
Noori

Optics Technical Department, Dijla
University College

Email: zaidoon.tariq@duc.edu.iq

زيدون طارق محمد نوري

كلية دجلة الجامعة - قسم تقنيات البصريات

Structural and optical properties of TiO₂/Fe₂O₃ nano crystalline thin film by pulsed laser deposition

محضر بالتريسيب ليزر النبض TiO₂ / Fe₂O₃ دراسة الخصائص الهيكلية والبصرية لغشاء نانو

Abstract

Nano TiO₂/Fe₂O₃ thin film with different concentrations 0.1, 0.3, 0.5 and 0.7, of TiO₂ were deposited by pulsed laser deposition technique on glass substrate. The optical constants such as (refractive index n , dielectric constant ϵ_i and Extinction coefficient κ) of the deposition films were obtained from the analysis of the experimental recorded the optical transmission of TiO₂/Fe₂O₃ thin films with thickness 150nm spectral data. The optical band gap of TiO₂/Fe₂O₃ films is calculated from $(\alpha h\nu)^2$ vs. photon energy curve. The optical band gap of the TiO₂/Fe₂O₃ films was found to be in the range 3.3 to 4 eV and the band gap decreases with increase TiO₂ content of the film.

الخلاصة :

رُسبت أغشية رقيقة من TiO₂/Fe₂O₃ لتراكيز مختلفة 0.1، 0.3، 0.5، 0.7 من TiO₂ بتقنية الترسيب بالليزر النبضي على أرضية من الزجاج. درست الثوابت البصرية مثل (معامل الانكسار n)، ثابت العزل الحقيقي والخيالي (ϵ_i, ϵ_r) ومعامل الخمود (κ) للأغشية المترسبة من تحليل طيف النفاذية. حسبت فجوة الطاقة البصرية لأغشية TiO₂/Fe₂O₃ من منحنى $(\alpha h\nu)^2$ مع طاقة الفوتون. وقيم فجوة الطاقة تتناقص بزيادة نسبة TiO₂ وكانت فجوة الطاقة لهذه الأغشية تتغير (من 3.3 إلى 4) إلكترون فولت.